www.lajss.org
Latin American Journal of Solids and Structures 2 (2005) 237–251

Three-dimensional Langmuir circulations and enhanced turbulence in upper mixed ocean layers

M. Araujo[a,*], D. Dartus[b], L. Masbernat[b] and Ph. Maurel[c]

[a]Laboratório de Oceanografia Física Estuarina e Costeira, Departamento de Oceanografia da Universidade Federal de Pernambuco, 50740-550, Recife–PE, Brasil
[b]Institut de Mécanique des Fluides de Toulouse – IMFT , U.M.R. CNRS/INP-UPS 5502, Allée du Professeur Camille Soula - 31400 Toulouse, France
[c]Institut Français du Pétrole - IFP, 1 et 4 Avenue de Bois-Préau, 92852 Rueil-Malmaison Cedex, France

Abstract

Field and laboratory data confirm the presence of longitudinal billows in fluid flow under wind-wavy surfaces. In the ocean these vortices (called Langmuir cells) act by mixing nutrients and other biological material, and thus their role cannot be neglected in vertical transfer modelling. In this work, non-dimensional mean velocity field equations are formulated with Craik & Leibovich theory, including interaction terms between surface wave Stokes drift and mean current. A first order turbulence closure model (k,ε) is used to model the Reynolds stress tensor. The model is formulated in non-dimensional grounds, and numerical experiments are performed using a finit-volume technique. In the first set of simulations, model outputs are compared to measurements obtained at three different laboratory wind-water facilities (Cheung & Street, 1988; Thais & Magnaudet, 1996). Results suggest that the presence of secondary motions is necessary for explaining the observed channel flows. A second group of simulations involves field situations, when numerical results are compared to some typical environmental cases (Kitaigorodskii et al., 1983). Model results for this second group of experiments show $\frac{\hat{k}}{u_*^2} = O\left(10^2\right)$ ($\hat{k}$ is the surface turbulent kinetic energy, and u_* is the water friction velocity), representing the same order of magnitude currently found in situ for turbulence.

1 Introduction

One exciting research field over the past twenty years is the increasing interaction between observationalists and modelers, with possibilities for predictions originating in either group being checked by the other. Wind-induced flow in presence of surface gravity waves is surely one of the the most important type of flow in geophysical situations. As a result, it has been widely studied by laboratory experiments and numerical models, although it is interesting to verify that works involving direct comparison between laboratory dataset and numerical simulations of Langmuir circulations are not very common. Most of previous works involve in particular a

*Corresp. author Email: moa@ufpe.br Received 26 September 2005; In revised form 10 October 2005

mathematical analysis of Langmuir cells' dynamics, followed sometimes by a small number of qualitative comparisons with field observations.

Langmuir circulations (hereafter referred to as LCs) are large-scale, organized convective motions in the surface layers of the natural systems. LCs are typically of larger horizontal scale than thermally driven convective instabilities, and exist under both thermally stable and thermally unstable conditions. Downwelling velocities approaching 1 % of the wind speed and the large scale of LCs suggest that this phenomenon can be a powerful mixing mechanism acting in the upper surface layers of lakes and oceans (Fig. 1).

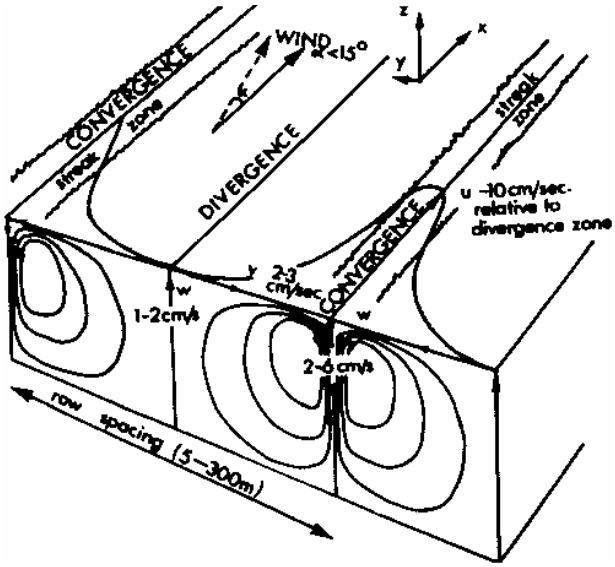

Figure 1: Main features of Langmuir circulations observed at surface layers of natural ecosystems. From [21].

One may separate the efforts in modelling LCs in two groups, according to the framework used. Firstly we have the spectral approach, which may be represented by the global/energetic and linear instability analysis (see Craik [9] and Leibovich [14], for inviscid non conductive fluid; Leibovich and Paolucci [16], for nonzero diffusivities fluid), and by the studies of nonlinear dynamics of LCs (see Leibovich *et al.* [15] and Cox *et al.* [7], for analogous Langmuir-thermosolutal convection problem; Li and Garrett [18, 19], for the investigation of the main flow structures). A second group of modelling efforts is reported to the local method simulations, based on the space and time discretisations of Craik-Leibovich equations. Earlier works from Leibovich [14], Leibovich and Paolucci [16] used finite-difference formulation to explore the time evolution of LCs at constant density water of infinite depth. Lele [17] performed the simulations with the same computer code by considering a constant vertical stratification or a preexisting stronger thermocline on the water column. He showed the importance of buoyancy effects on limiting the vertical penetration of convective motions.

All these previous theoretical and modeling studies take account of a turbulence closure based on constant eddy viscosity. This simpler approach was a priori justified by the diffusive role of the turbulence, which should not be at the origin of LCs generation. Meanwhile, it caused a greater restraint because simulation results were strictly depending upon initial eddy viscosity estimation. Recent large-eddy simulations (LES) by Skyllingstad and Denbo [23] yield to bear out some theoretical and experimental insights about LCs dynamics. In the LES approach a separation between these motions does not exist until the sub-grid scale resolution, although estimation of sub-grid eddy viscosity remains a problem.

Laboratory facilities were currently used as a way of allowing more controlled analysis about wave-mean current and wave-turbulence interactions. Different forms of wind-wave generation and flow condition have been studied. Experiences conducted by Prodhomme [22] and Thais [24] (hereafter referred to as PRT), at the wind-wave tunnel of the *Institut de Mécanique des Fluides de Toulouse*, have shown the fundamental implication of wave-induced convection like LCs over the flows' dynamics. On the other hand, Thais and Magnaudet [26] (hereafter refered to as TH) carried out a set of experiences at the larger wind-wave tunnel of the *Institut de Mécanique Statistique et de la Turbulence de Marseille*, giving some indications about the existence of a wave-enhanced region beneath surface flow where the turbulence and dissipation rates reach one order of magnitude greater than in a comparable turbulent boundary layer.

These laboratory data support earlier lake and ocean measurements. Field data obtained at Lake Ontario's platform by Kitaigorodskii *et al.* [12] and Agrawal *et al.* [1] show values of turbulent kinetic energy up to 20 times greater than those normally found near wall layers, as well as dissipation rates up to 70 times greater than its corresponding wall values. An analogous behaviour for dissipation rates in the ocean is reported in Gargett's [11] review. Furthermore, Thais' experiences confirm the importance of the balance between diffusion and dissipation of turbulent kinetic energy near surface. In the presence of breaking waves, shear production and dissipation of turbulence no longer balance, and the classical law of the wall does not apply. Similar conclusions were obtained by Craig and Banner [8] using laboratory data of Cheung and Street [5, 6] (hereafter referred to as CS).

The aim of this paper is to evaluate two little studied phenomena simultaneously found in geophysical water flows: the wave-mean current interactions, which are responsible for the presence of secondary motions like Langmuir circulations; and the high enhanced turbulence levels observed beneath wind-wave surfaces. Data collected from three different laboratory facilities were initially used to identify length and velocity scales for data assemblage. A full modelling system of Reynolds equations is proposed. The need to consider secondary motions (LCs) to obtain the experimental flows dynamics is shown. A second group of simulations involves field situations, when numerical results are compared to typical environmental cases.

2 Experimental dataset

The initial part of this study is centred on three datasets collected by CS in Stanford University, by PRT at the *Institut de Mécanique des Fluides de Toulouse*, and by TH at the *Institut de Mécanique Statistique et de la Turbulence de Marseille*. Stanford experiences were conducted at a wind-wave tunnel of 1.9 m high (water about 1 m deep), 0.9 m wide, 35 m long and a single measurements fetch of 13 m from the beginning of the channel (see Cheung and Street [5, 6] for detailed description of experimental set-up). Experiments were run at seven discrete wind speeds from 1.5 to 13.1 m.s^{-1}, but the lowest two speeds appeared not to clearly create fully developed turbulent boundary layers, and only speeds of 4.7 m.s^{-1}and higher are considered in the present study. The Toulouse wind-wave tunnel also has a test section also about 13 m from the channel inlet, which is 1.2 m wide and 2.0 m high (water 1 m deep). In this case, a closed circuit system keeps a liquid mean flow 20 to 26 l.s^{-1}. The experiments were conducted at seven wind speed from 3.8 to 13.5 m.s $^{-1}$, but only speeds of 4.5 m.s^{-1}and higher were considered here (see e.g., Prodhomme [22] for detailed experimental set-up). The third dataset (Marseille) was carried out in a larger air-sea facility, composed of a closed channel with dimensions of 40 m long, 2.6 m high and 3.2 m wide. During experiences mean water depth was 0.9 m and a single downstream section of measurements were placed at a fetch of 26 m from the channel inlet. Three air free-stream velocities are 4.5 m.s^{-1}, 5.9 m.s^{-1} and 7.8 m.s^{-1}.

For all datasets, the mean streamwise air velocity profile was determined with a Pitot static tube; water-surface elevation was determined by the use of capacitance wave-height gauges, and a two-component laser-Doppler-anemometer (LDA) system was used in the forward-scatter mode to determine the longitudinal and vertical components of the velocity in the water. Friction velocities (u_{*i}) were determined by CS directly from shear stress measurements in the water, and PR and TH calculated air friction velocities for applying interface turbulent shear stress continuity in u_{*i}estimation. Stanford's and Marseille's data are reported to vertical profile measurements collected from a single section situated at channel axis ($y = 0.0\ m$).

Data post-processing included the determination of longitudinal (u) and vertical velocities (w) (mean and fluctuation parts), turbulent kinetic energy (k), turbulent shear stress ($-\overline{u'w'}$), and predominating wave parameters (obtained from wave spectra). For wave and turbulent decomposition two distinct separation schemes were used. PRT and CS have employed the linear method proposed by Belinov *et al.* [4], whereas more energetic waves of TH were treated with triple decomposition method (Thais and Magnaudet [25]). Table 1 presents the main features of laboratory flows considered in simulations. KI denotes the field experiences performed by Kitaigorodskii *et al.* [12] at Lake Ontario, Canada.

Table 1: Main features of laboratory flows considered in simulations.

Flow name	Wind velocity ($m.s^{-1}$)	Wave pulsation ($rad.s^{-1}$)	Wave number k_W (m^{-1})	Wave ampl. a (m)	Longitudinal mean flow ($m.s^{-1}$)	Channel *Fetch* (m)	Channel width L (m)	Water depth d(m)
CS67	6.7	13.87	19.63	0.008	-	13.00	0.92	0.97
CS99	9.9	11.71	13.98	0.012	-	13.00	0.92	0.97
PRT9	9.0	10.90	17.75	0.011	0.017	13.95	1.20	1.00
PRT13	13.5	8.68	11.86	0.020	0.017	13.95	1.20	1.00
TH6	5.9	11.35	13.51	0.013	-	26.00	2.60	0.90
TH8	7.8	9.99	11.18	0.018	-	26.00	2.60	0.90
KI6	6.1	2.62	0.70	0.115	-	1100.00	12.50	12.50
KI11	10.7/11.2	3.58	1.30	0.093	-	1100.00	12.50	12.50

3 Model equations and finit-volume method

3.1 Governing equations

Governing equations allow simultaneous analysis of secondary mean flows and turbulence parameters. The three velocity components u, v, w represent the downwind (x-longitudinal axis), crosswind (y-horizontal spanwise axis, origin situated at channel axis) and vertical velocities (z-vertical axis, upward from surface origin). All flows treated are steady, homogeneous in density, and fully developed in longitudinal direction; the secondary cells will be placed at (y-z) plane (see Fig. 1).

The choice of nondimensionalizing scales was made after a previous analysis of experimental dataset, since it is appropriate to use reference scales that allow a best assemblage of wind-tunnel measurements (dimensional quantities are written thereafter under *small hats*). Inverse wave number was used as spatial reference, and mean velocities were normalized by $u_* = \sqrt{\tau_S/\rho}$, the water friction velocity related to a constant wind stress τ_i and water density ρ. All flows treated in simulations are fully developed in longitudinal direction, resulting in constant pressure gradient in this direction.

Normalisation scales for turbulent kinetic energy and dissipation rates were chosen after many attempts in grouping experimental measurements. *Prandt-Kolmogorov* formulae was then used for eddy viscosity. Mean flow and turbulent equations take the following form :

$$x = k_W \hat{x} \quad ; \quad u = \hat{u}/u_* \quad ; \quad v = \hat{v}/u_* \quad ; \quad w = \hat{w}/u_* \tag{1}$$

$$\alpha^* = \frac{(\partial \hat{p}/\partial \hat{x})}{\rho k_W u_*^2} \quad ; \quad k = \frac{\hat{k}}{u_*^2} \quad ; \quad \varepsilon = \frac{\hat{\varepsilon}}{k_W u_*^3} \tag{2}$$

$$\frac{\partial v}{\partial y} + \frac{\partial w}{\partial z} = 0 \tag{3}$$

$$v\frac{\partial u}{\partial y} + w\frac{\partial u}{\partial z} = -\alpha^* + \frac{\partial}{\partial y}\left(\nu_t \frac{\partial u}{\partial y}\right) + \frac{\partial}{\partial z}\left(\nu_t \frac{\partial u}{\partial z}\right) + \frac{\partial}{\partial z}\left(-\overline{\tilde{u}\tilde{w}}\right) \tag{4}$$

$$v\frac{\partial v}{\partial y} + w\frac{\partial v}{\partial z} = -\frac{\partial p_1}{\partial y} + \frac{\partial}{\partial y}\left(\nu_t \frac{\partial v}{\partial y}\right) + \frac{\partial}{\partial z}\left(\nu_t \frac{\partial v}{\partial z}\right) + S_V \tag{5}$$

$$v\frac{\partial w}{\partial y} + w\frac{\partial w}{\partial z} = -\frac{\partial p_1}{\partial z} + \frac{\partial}{\partial y}\left(\nu_t \frac{\partial w}{\partial y}\right) + \frac{\partial}{\partial z}\left(\nu_t \frac{\partial w}{\partial z}\right) + S_W \tag{6}$$

$$v\frac{\partial k}{\partial y} + w\frac{\partial k}{\partial z} = \frac{\partial}{\partial y}\left(\frac{\nu_t}{\sigma_k}\frac{\partial k}{\partial y}\right) + \frac{\partial}{\partial z}\left(\frac{\nu_t}{\sigma_k}\frac{\partial k}{\partial z}\right) + Pr - \varepsilon \tag{7}$$

$$v\frac{\partial \varepsilon}{\partial y} + w\frac{\partial \varepsilon}{\partial z} = \frac{\partial}{\partial y}\left(\frac{\nu_t}{\sigma_\varepsilon}\frac{\partial \varepsilon}{\partial y}\right) + \frac{\partial}{\partial z}\left(\frac{\nu_t}{\sigma_\varepsilon}\frac{\partial \varepsilon}{\partial z}\right) + C_{1\varepsilon}\frac{\varepsilon}{k}Pr - C_{2\varepsilon}\frac{\varepsilon^2}{k} \tag{8}$$

in which k_W is the characteristic wave number of the surface wave spectrum, $\mathrm{k} = \frac{1}{2}\left(\overline{\mathrm{u}'^2} + \overline{\mathrm{v}'^2} + \overline{\mathrm{w}'^2}\right)$ is the turbulent kinetic energy, $\varepsilon = \nu\overline{\nabla \mathbf{v}'.\nabla \mathbf{v}'}$ is the dissipation rate, and $\nu_t = \frac{\hat{\nu}_t k}{u_*} = C_\mu \frac{\mathrm{k}^2}{\varepsilon}$ is the eddy viscosity. C_μ, σ_k, σ_ε, $C_{\varepsilon 1}$, $C_{\varepsilon 2}$ (0.09, 1.0, 1.3, 1.44, 1.92) are the standard constants of the $(\mathrm{k}-\varepsilon)$ model.

In equations (4) to (6), the turbulent flux of momentum obey the *Boussinesq* assumption, written in *Einstein* frame as :

$$\begin{cases} S_{ij} = \frac{1}{2}\left(\frac{\partial \mathrm{v}_i}{\partial \mathrm{x}_j} + \frac{\partial \mathrm{v}_j}{\partial \mathrm{x}_i}\right) \\ -\overline{\mathrm{v}'_i \mathrm{v}'_j} = 2\, S_{ij}\nu_t - \frac{2}{3}\mathrm{k}\,\delta_{ij} \end{cases} \tag{9}$$

The last right side terms of v and w momentum equations give us the wave-mean current interactions (Craik-Leibovich terms), supporting Langmuir cells :

$$\begin{cases} S_U = u_S \frac{\partial u}{\partial y} \\ S_W = u_S \frac{\partial u}{\partial z} \end{cases} \tag{10}$$

The production term in (7) and (8) writes in first order approximation for homogeneous longitudinal flows as :

$$\mathrm{Pr} = \nu_t \left[\left(\frac{\partial \mathrm{u}}{\partial \mathrm{y}}\right)^2 + \left(\frac{\partial \mathrm{u}}{\partial \mathrm{z}}\right)^2 + \left(\frac{\partial \mathrm{v}}{\partial \mathrm{z}} + \frac{\partial \mathrm{w}}{\partial \mathrm{y}}\right)^2 + 2\left(\frac{\partial \mathrm{v}}{\partial \mathrm{y}}\right)^2 + 2\left(\frac{\partial \mathrm{w}}{\partial \mathrm{z}}\right)^2\right] \tag{11}$$

The nondimensional Stokes drift current u_S is obtained from the Airy's solution for a monochromatic wave field :

$$\mathrm{u}_S = \frac{a^2 k\sigma}{u_*}\frac{cosh\,(\mathrm{z} + \mathrm{N}_h)}{2\,sinh^2\,(\mathrm{N}_h)} \tag{12}$$

where $\mathrm{N}_h = k\,d$ (d is the water depth in channel flume).

3.2 Boundary conditions

The nondimensional boundary conditions at the bottom are imposed at the logarithmic zone near the wall. So we have at $z = -N_h + k\delta_W$ ($50 \leq \frac{u_{*W}\,\delta_W}{\nu} \leq 150$,$u_{*W}$ and v_{*W} denote the wall friction velocities at the bottom, and ν is the water kinematical viscosity) for momentum and turbulence equations :

$$u_w = R\left(\frac{1}{\chi}\ln\delta_W^+ + 5.5\right); \quad \mathrm{v}_W = \mathrm{R}\left(\frac{v_{*W}}{u_{*W}}\right)\left[\frac{1}{\chi} ln\left(\delta_W + \frac{v_{*W}}{u_{*W}}\right) + 5.5\right] \quad ; \quad \mathrm{w}_W = 0 \tag{13a}$$

$$\mathrm{k}_W = \mathrm{R}\ C_\mu^{-1/2} \quad ; \quad \varepsilon_W = \frac{\mathrm{R}^{3/2}}{\chi\ k_W\ \delta_W} \tag{13b}$$

where χ is the *von Karman* constant, and $\mathrm{R} = \frac{\tau_W}{\tau_S}$ is the ratio between the bottom wall and the wind induced stress at surface.

All simulations were performed adopting an integration domain that corresponds to a half-width for each experimental channel (L/2). Symmetrical boundary conditions were imposed at each lateral side of this domain ($y = 0$ and $y = kL/2$), which is mathematically represented by :

$$\frac{\partial \mathrm{u}}{\partial \mathrm{y}} = \frac{\partial \mathrm{v}}{\partial \mathrm{y}} = \frac{\partial \mathrm{w}}{\partial \mathrm{y}} = 0 \tag{14}$$

Surface boundary conditions have strong influences over the flow dynamics. The small values of longitudinal mean flows and the low levels of turbulence shear production at the channel's bottom contribute to the importance of the surface conditions. For the velocity components a wind induced longitudinal shear stress is applied, associated to a zero longitudinal mean vorticity. These conditions are imposed at $z = -\mathrm{N}_h + k\delta_P$ ($50 \leq \frac{u_*\,\delta_S}{\nu} \leq 150$, the subscript s is used to indicate the surface) and may be written in nondimensional grounds as:

$$\nu_t\ \frac{\partial \mathrm{u}}{\partial \mathrm{z}}\bigg|_S = 1 \quad ; \quad \frac{\partial \mathrm{v}}{\partial \mathrm{z}}\bigg|_S = 0 \quad ; \quad \mathrm{w}_S = 0 \tag{15}$$

The surface boundary condition on turbulent kinetic energy and dissipation rate should introduce the influence of surface waves, as follows :

$$\frac{\partial \mathrm{k}}{\partial \mathrm{z}}\bigg|_S = 2\ \mathrm{k}_S\, exp\,(2\,\mathrm{z}) \quad ; \quad \frac{\partial \varepsilon}{\partial \mathrm{z}}\bigg|_S = 6\left(\frac{3}{2}\frac{C_\mu}{\sigma_k}\right)^{1/2} \mathrm{k}_S^{3/2}\, exp\,(3\,\mathrm{z}) \tag{16}$$

Values of k_S in (16) were obtained from the equation proposed in Araujo *et al.* [3], in the form:

$$\mathrm{k}_S = 0.12\ \left(\frac{\sigma a}{u_*}\right)^2 + C_\mu^{-1/2} \tag{17}$$

3.3 Finit-volume method

The set of equations (1)-(8) with boundary conditions (13)-(16) is solved numerically. The model uses a finite volume method with a classical staggered grid, where pressure is solved in the center of each control volume and velocities at cell surfaces. Unsteady terms are discretized using a fully implicit scheme. Convective terms use the Hybrid scheme which consists of a centred scheme for local *Peclet* numbers (Pe) between -2 and 2 and an upwind scheme outside this interval. The SIMPLEST algorithm (Patankar [20]) is used to solve the resulting set of discretized linear algebraic equations. It interactively adjusts an assumed pressure field by successive pressure corrections in order to allow the resulting estimated velocity field to satisfy the mass continuity equation. Bottom friction velocities are calculated interactively by the code, and the longitudinal pressure gradient is adjusted in order to satisfy the mean longitudinal velocity (u_R). Convergence is reached when the mass imbalance in each cell falls below the chosen threshold (herein 0.01 % of the mass cell is used).

The spatial grid step is regular in the y-direction and a progressive small mesh size is used in the z-direction near the bottom wall and the flow surface. Typical simulations have about 100 by 100 to 200 by 200 number of cells. Aspect ratios $\Delta y/\Delta z$ between horizontal and vertical mesh sizes change from 1.5 for vertical boundary regions to 1.0 in central flow zones. The number and distribution of control volumes (for each simulation case) were chosen after considering different sizes of integration domains, as well as after a minimal number of preliminary tests. Steady numerical simulations were performed until two key variables, pitch (Pi) introduced by Li and Garrett [7] and the maximum downwelling vertical velocity (w_{dn}), representing flow dynamics, remained constant for two successive grid configurations (Araujo [2]).

All boundary conditions are implemented in the code by adding complementary terms to the discrete equations in adequate control volumes. In the vorticity generation terms S_V and S_W in (11), the Stokes drift is evaluated in each vertical coordinate from its analytical expression (12) and centered-difference formulae is used for $\partial u/\partial y$ and $\partial u/\partial z$.

4 Numerical results and Discussion

4.1 Laboratory experiments – Stanford, Toulouse and Marseille

Figures 2 to 5 provide the laboratory modelling set of results. Fig. 2 is reported to experiences carried out by CS at Stanford. Fig. 4 presents the data obtained by PRT at Toulouse, and Fig. 5 brings the results obtained for more energy waves cases TH in Marseille. These figures are referred to distinct couples of surface forcings. These surface forcings are represented by different wind speed and wave parameters (Tab. 1). Model outputs for longitudinal mean velocity (u) and Turbulent Kinetics Energy – TKE (k) are compared to experimental profiles. They are reported to vertical profiles of longitudinal mean currents obtained at the channel axis ($y = 0$), where vertical upwelling velocities were measured. For each study case two numerical results

are plotted in Figs. 2 to 5, as follows :

- the classical parallel flow, obtained without the Craik-Leibovich terms (4) in the righthand sides of equations (5) and (6). This situation corresponds to *Couette* flow and is represented by dashed profiles in all figures;
- the flow in the presence of secondary motions (Langmuir cells), which develops when Craik-Leibovich source terms (10) are take into account for simulations. These results are represented by full line profiles in all figures.

These findings show net differences between cell presence flows and those parallel situations. All cases show a remarkable influence of vertical convection over momentum profiles. The presence of convective cells provokes a net reduction of surface entrainment, which is well reproduced in model simulations. These reductions in surface momentum transfer could be initially explained if we suppose that the boundary condition for longitudinal momentum (14) is not satisfactory. Wu [28], remarks that some part of wind produced momentum is used for wave development, and that only the remaining part is transferred to the water (It should be equivalent to a surface condition given by $\nu_t \left.\frac{\partial \mathrm{u}}{\partial \mathrm{z}}\right|_S = \gamma\ 1$, where $0 < \gamma < 1$). Another possible explanation is associated to the wave-breaking process, which is commonly observed for high wave-slopes (e.g., geophysical ocean situations). Previous simulations tests performed by using Wu's conditions (for different values of γ) did not produce satisfactory results, and in the same way there was no observed significant wave-breaking process during the experiments, which is in agreement with the small values of generated wave-slopes (Tab. 1).

In order to examine the longitudinal momentum balance when convection cells are present or absent, the normalized components of longitudinal mean momentum Eq. (4) can be redefined as follows :

$$-\left(\mathrm{v}\frac{\partial \mathrm{u}}{\partial \mathrm{y}} + \mathrm{w}\frac{\partial \mathrm{u}}{\partial \mathrm{z}}\right) - \alpha^* + \frac{\partial}{\partial \mathrm{y}}\left(-\overline{u'v'}\right) + \frac{\partial}{\partial \mathrm{z}}\left(-\overline{u'w'}\right) = 0 \tag{18}$$

Figure 3 shows the typical vertical distributions of momentum terms at the central axis upwelling region, where positive upward vertical velocities were observed. This figure also presents momentum equilibrium for parallel flow.

The left side in Fig. 3 shows a single classical situation observed in parallel flow which assures that the pressure gradient term $-\alpha^*$ is equilibrated by turbulent diffusion. Nevertheless the presence of vertical convection imposes different momentum distributions within the channel cross-section. In this case, central channel upwelling region profiles in the righthand side of Fig. 3 show a general equilibrium between secondary convection and diffusion of momentum, which was observed in all simulated cases. In this region, we have $\mathrm{v}\partial \mathrm{u}/\partial \mathrm{y} \approx 0$ as a result of symmetrical boundary conditions – (9). Results indicate that vertical diffusion is greater then secondary convection, this difference is then basically compensated by pressure gradient considering that lateral diffusion is always positive in this region. Calculated vertical profiles of momentum go to zero near the surface as a result of the absence of vertical convection closer to the surface.

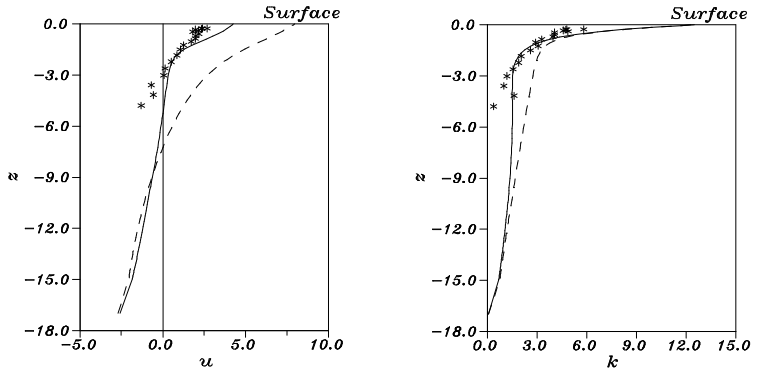

(a)

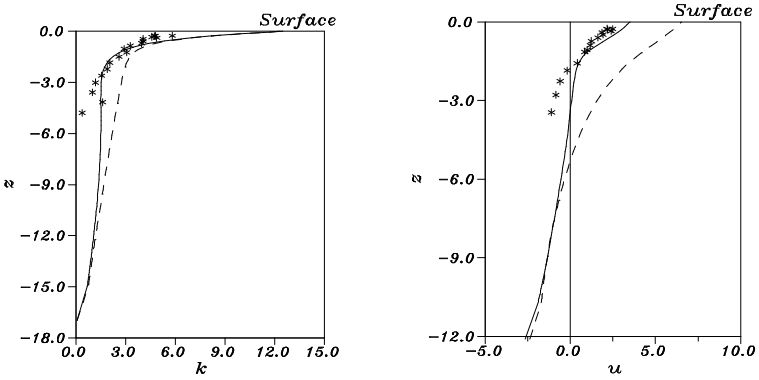

(b)

Figure 2: Longitudinal mean velocity (u) and TKE (k) at Stanford for (a) CS67 and (b) CS99. (*) Laboratory ; (——) Model secondary flow ; (– – –) Model parallel flow

Another remarkable aspect induced by the presence of Langmuir circulations relates to the influence of convective motions over the spatial distribution of turbulent shear stress, and in consequence the spatial distribution of turbulence. In Figs. 2, 4 and 5 we verify the influences of the non-linearity of vertical turbulent shear stress over TKE distribution in presence of secondary flows. Lower TKE intensity levels at the central part of the flow (along depth) are obtained in all study cases.

4.2 Field experiments – Lake Ontario, Canada

The second group of simulation reports data for two environmental cases collected by Kitaigorodskii *et al.* [24] in Lake Ontario, Canada. Wind and wave characteristics are presented in Tab. 1). They relate to mean wind forces, wave height (2a) and frequency (σp. Wave numbers (k_W) in Tab. 1 were calculated from the dispersion relation.

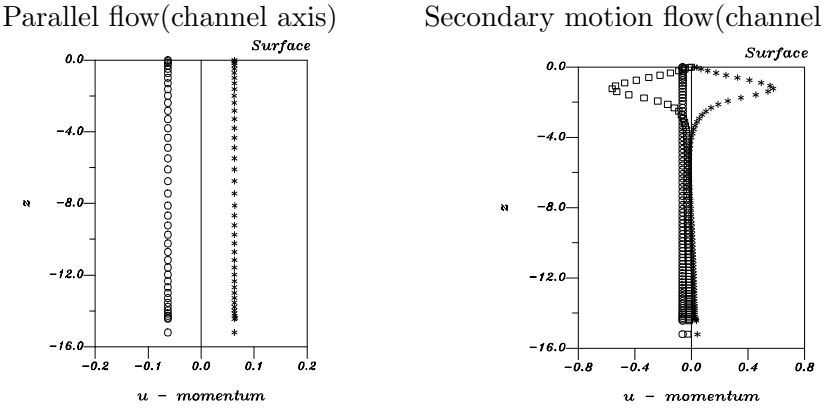

Figure 3: Balance of longitudinal momentum at the channel axis. Comparison between parallel situation and the flow in the presence of upwelling secondary motions :
(*) $\frac{\partial}{\partial \mathrm{y}}\left(-\overline{u'v'}\right)$; ($^\circ$) $-\alpha^*$; (□) $-\left(\mathrm{v}\frac{\partial \mathrm{u}}{\partial \mathrm{y}}+\mathrm{w}\frac{\partial \mathrm{u}}{\partial \mathrm{z}}\right)$; (———) balance.

In Fig. 6 we compare field TKE data with the numerical profiles for KI6 and KI11 flows.

Results indicate that the model proposed herein (including LCs generation terms) is capable of reproducing lake measurements.

Nevertheless, the big issue in Fig. 6 is the observed and simulated values of TKE beneath the air-water interface. In KI6 (left side in Fig. 6) we have near surface $k=\frac{k}{u_*^2}=O\left(150\right)$, while KI11 (right side) simulation yields $k=\frac{k}{u_*^2}=O\left(60\right)$. These values are about 50-fold and 20-fold higher (respectively) than the classical boundary layer values currently measured near a sheared wall (Klebanoff [13]). These results are in agreement with some recent field measurements that have confirmed the existence of a turbulence enhanced sublayer of a depth approximately 10 times the wave amplitude (Drennan *et al.* [10]; Agrawal *et al.* [1]; Thorpe [27]).

5 Conclusions

The most used approach to study the vertical dynamics of upper ocean mixed layers is the deployment of vertical one-dimensional models, in which the lateral distribution of mass, momentum and energy are considered unimportant. This approach has long been supported by the greater interest in understanding the influence of momentum over the biotic components in photic productive regions of surface waters. These models are normally limited to the use of semi-empirical laws for representing vertical diffusivities, where global analytical formulations for vertical diffusion coefficients are considered.

In this work we show that induced vertical motions beneath wind-wavy surfaces have strong influences over flow dynamics and cannot be neglected in vertical transfer modelling. This ver-

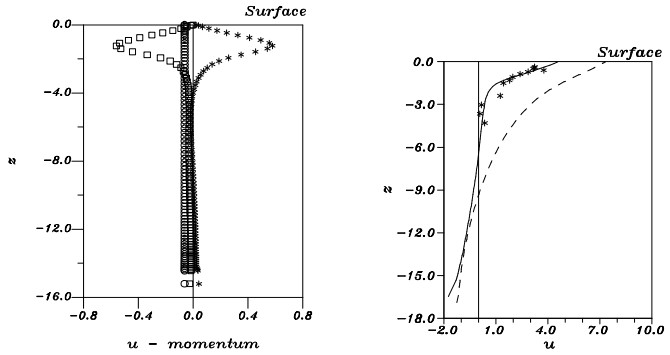

(a)

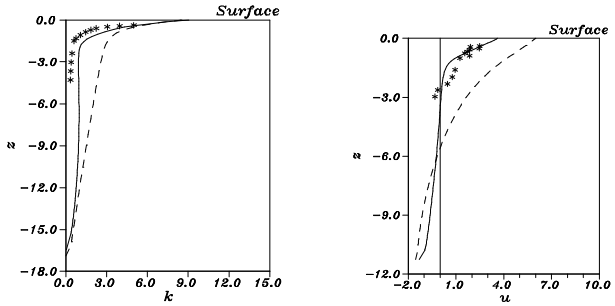

(b)

Figure 4: Longitudinal mean velocity (u) and TKE (k) at Toulouse for : (a) PRT8 and (b) PRT13. (*) Laboratory ; (——) Model secondary flow ; (– – –) Model parallel flow.

tical convection may be associated to the presence of cross-wind cells like Langmuir circulations (LCs).

In order to evaluate the effects of LCs over the vertical distribution of momentum and energy, two groups of numerical simulations were carried out. In the first set of simulations, model outputs are compared to measurements obtained at three different laboratory wind-water facilities. Simulation outputs were systematically compared with available flow measurements. We report to model results for two distinct situations: simple parallel *Couette* flow, and with the introduction of wave-currents interaction terms, giving rise to mechanical secondary cells. Model results for simulations taking account the mechanical interaction of wave-currents show good correspondence with measurements, suggesting the presence of Langmuir cells as a prime factor to explain observed flow structures.

The second group of simulations involved field situations, and numerical profiles were compared to two typical environmental cases. Model results for this second group of experiments show $\frac{\hat{k}}{u_*^2} = O\left(10^2\right)$. This last evidence has remarkable consequences: (a) first, it confirms the high levels of turbulent kinetic energy recently measured in the ocean, and (b) second, it points out the prime importance of turbulence diffusion over the vertical transport of particulate and

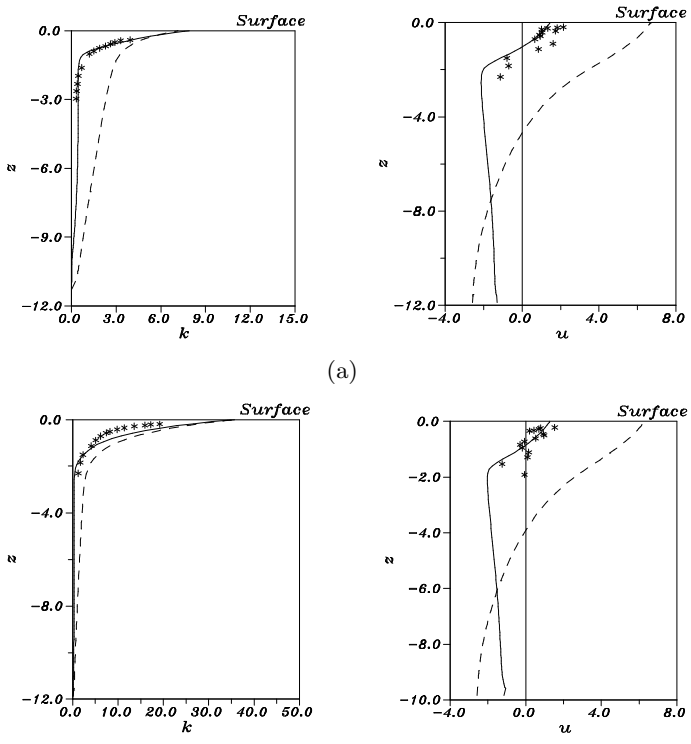

Figure 5: Longitudinal mean velocity (u) and TKE (k) at Marseille for : (a) TH6 and (b) TH8. (*) Laboratory ; (——) Model secondary flow ; (– – –) Model parallel flow.

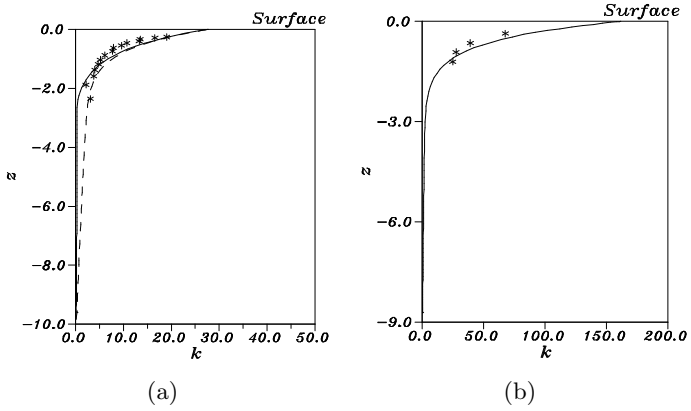

Figure 6: TKE (k) at Lake Ontario for : (a) KI6 and (b) KI11. (*) Field data ; (——) Model secondary flow.

dissolved constituents within the upper mixed layer of natural systems.

References

[1] Y. C. Agrawal, E. A. Terray, M. A Donelan, P. A. Hwang, A. J. Williams, W. M. Drennan, K. K. Kahma, and S. A. Kitaïgododskii. *Enhanced Dissipation of Kinetic Energy beneath Surface Waves*, volume 359. Nature, 1992.

[2] M. Araujo. *Circulations de Langmuir et Turbulence sous une Houle Cisaillée par le Vent*. PhD thesis, Institut National Polytechnique de Toulouse, 1996.

[3] M. Araujo, D. Dartus, Ph. Maurel, and L. Masbernat. Langmuir circulations and enhanced turbulence benath wind-waves. *Ocean Modelling*, 3:109–126, 2001.

[4] A. Y. Belinov, O. A. Kouznetsov, and G. N. Panin. On the analysis of wind-wave induced disturbances in the atmospheric turbulent surface layer. *Bound. Layer Met.*, 6:269–285, 1974.

[5] T. K. Cheung and R. L. Street. Turbulent layer in the water at an air-water interface. *J. Fluid Mech.*, 194:133–151, 1988.

[6] T. K. Cheung and R. L. Street. Wave-following measurements in the water beneath an air-water interface. *J. Geophys. Res.*, 93:14089–14093, 1988.

[7] S. M. Cox, S. Leibovich, I. M. Moroz, and A. Tandon. Nonlinear dynamics in langmuir circulations with o(2) symmetry. *J. Fluid Mech.*, 241:669–704, 1992.

[8] P. D. Craig and M. L. Banner. Modelling wave-enhanced turbulence in the ocean surface layer. *J. Phys. Ocean.*, 24:2546–2559, 1996.

[9] A. D. D. Craik. The generation of langmuir circulations by an instability mechanism. *J. Fluid Mech.*, 125:37–52, 1977.

[10] W. M. Drennan, K. K. Kahma, E. A. Terray, M. A. Donelan, and S. A. Kitaigorodskii. *Observations of Enhancement of Kinetic Energy Dissipation beneath Breaking Wind Waves. In M. L. Banner and R. H. J. Grimshaw, eds., Breaking Waves*. Springer, 1992.

[11] A. E. Gargett. Ocean turbulence. *Ann. Rev. Fluid Mech.*, 21:419–451, 1989.

[12] S. A. Kitaigorodskii, M. A. Donelan, J. L. Lumley, and E. A. Terray. Wave-turbulence interactions in upper ocean. part ii: Statistical characteristics of wave and turbulent components of the random velocity field in the marine surface layer. *J. Phys. Ocean.*, 13:1988–1999, 1983.

[13] P. S. Klebanoff. *Characteristics of Turbulence in a Boundary Layer Flow with zero Pressure Gradient*. Nat. Acad. Scien. Rep., USA, 1955.

[14] S. Leibovich. Convective instability of stably stratified water in the ocean. *J. Fluid Mech.*, 82:561–585, 1977.

[15] S. Leibovich, S. K. Lele, and I. M. Moroz. Nonlinear dynamics in langmuir circulations and in thermal convection. *J. Fluid Mech.*, 198:471–511, 1989.

[16] S. Leibovich and S. Paolucci. The instability of the ocean to langmuir circulation. *J. Fluid Mech.*, 102:141–167, 1981.

[17] S. K. Lele. *Some Problems in Hydrodynamic Stability arising in Geophysical Fluid Dynamics*. PhD thesis, Cornell University, 1985.

[18] M. Li and C. Garrett. Cell merging and the jet/downwelling ratio in langmuir circulations. *J. Mar. Res.*, 51:737–769, 1993.

[19] M. Li and C. Garrett. Is langmuir circulation driving by surface waves or surface cooling? *J. Phys. Ocean.*, 25:64–76, 1995.

[20] S. V. Patankar. *Numerical Heat Transfer and Fluid Flow*. Hemisphere Publis. Co., 1980.

[21] R. T. Pollard. *Observations and Theories of Langmuir Circulations and their Role in near Surface Mixing. In M. Angel, ed. A Voyage of Discovery : G. Deacon 70th Aniversary Volume*. Pergamon Press, 1977.

[22] M. T. Prodhomme. *Turbulence sous les Vagues de Vent*. PhD thesis, Institut National Polytechnique de Toulouse, 1988.

[23] E. D. Skyllingstad and D. W. Denbo. An ocean large-eddy simulation of langmuir circulations and convection in the surface mixed layer. *J. Geophys. Res.*, 100:8501–8522, 1995.

[24] L. Thais. *Contribution a l'Étude du Mouvement Turbulent sous des Vagues Cisaillées par le Vent*. PhD thesis, Institut National Polytechnique de Toulouse, 1994.

[25] L. Thais and J. Magnaudet. A triple decomposition of the fuctuating motion below laboratory wind water waves. *J. Geophys. Res.*, 100:741–755, 1995.

[26] L. Thais and J. Magnaudet. Turbulent structure beneath surface gravity waves sheared by wind. *J. Fluid Mech*, 328:313–344, 1996.

[27] S. A. Thorpe. Bubbles clouds and the dynamics of the upper ocean. *Quart. J. Royal Met. Soc.*, 118:1–22, 1992.

[28] J. Wu. Wind induced drift currents. *J. Fluid Mech.*, 68:49–70, 1975.